Journal of Materials Chemistry A

Copper Zinc Tin Sulfide as the Catalytic Materials for Counter Electrodes in Dye-Sensitized Solar Cells

Journal:	*Journal of Materials Chemistry A*
Manuscript ID:	TA-ART-05-2014-002319.R3
Article Type:	Paper
Date Submitted by the Author:	30-Aug-2014

Complete List of Authors:	Fan, Miao-Syuan; National Taiwan University, Department of Chemical Engineering Chen, Jian-Hao; Chang Gung University, Department of Chemical and Materials Engineering Li, Chun–Ting; National Taiwan University, Chemical Engineering Cheng, Kong-Wei; National Taiwan University, Department of Chemical Engineering Ho, Kuo-Chuan; National Taiwan University, Department of Chemical Engineering

Journal of Materials Chemistry A

Dynamic Article Links ►

Cite this: DOI: 10.1039/c0xx00000x

ARTICLE TYPE

www.rsc.org/xxxxxx

Copper Zinc Tin Sulfide as the Catalytic Materials for Counter Electrodes in Dye-Sensitized Solar Cells

Miao-Syuan Fan,[‡a] Jian-Hao Chen,[‡b] Chun-Ting Li,[a] Kong-Wei Cheng,[*b] and Kuo-Chuan Ho[*ac]

Received (in XXX, XXX) Xth XXXXXXXXX 20XX, Accepted Xth XXXXXXXXX 20XX
DOI: 10.1039/b000000x

The quaternary Cu_2ZnSnS_4 (CZTS) semiconductor thin films, deposited onto the indium-doped tin oxide (ITO) conducting substrate by sulfurizing the direct-current (DC) magnetron sputtered Cu-Zn-Sn metal alloys, were used as the counter electrode (CE) of dye–sensitized solar cells (DSSCs). X-ray diffraction (XRD) and Raman spectroscopy reveal that all of the samples are kesterite Cu_2ZnSnS_4 phase. The morphology becomes more smooth for the Cu-rich or Zn-rich sample, as judged by atomic force microscopy (AFM) and field–emission scanning electron microscopy (FE-SEM).The influence of the [Cu]/[Zn]+[Sn] molar ratio in the CZTS samples on the catalytic performance of DSSCs was also investigated. The electrocatalytic ability and electrochemical properties of the CEs were studied by cyclic voltammetry (CV), electrochemical impedance spectroscopy (EIS), and Tafel plot. The performance of DSSCs with various CEs was verified by *J–V* curves and incident photon–to–current conversion efficiency (IPCE) curves. The maximum solar-to-electrical power efficiency of DSSCs using the CZTS as the CE approached 7.94%. Those results show the attractive potential of CZTS to replace Pt CE (8.55%). The influence of different molar ratios of CZTS CEs on the DSSC performance was discussed in detail.

Introduction

Dye-sensitized solar cells (DSSCs) have been extensively studied in recently years, because of their attractive benefits such as high cell conversion efficiency, low cost and easy preparation procedures.[1-4] A typical DSSC is consisted of a nanocrystalline TiO_2 /dye photo-anode, electrolyte, and a counter electrode (CE). The counter electrode is an important component in DSSCs, because it collects the electrons from the external circuit and allows the I_3^- reduction reaction. The platinum (Pt) deposited onto a transparent conducting oxides (TCO) glass was the most commonly used CE due to its excellent electrocatalytic ability, chemical stability and electrical conductivity.[5,6] However, Pt is rather expensive, which limits its industrial applications. Searching for the low-cost substituted CEs for Pt is a major research in the development of practical DSSCs. Several electrocatalytic materials such as carbon-based materials[7,8], conducting polymers[9-11] and transition metal sulfides[12,13] have been extensively investigates. Recently, metal sulfides such as FeS_x[14,15], CoS[16-18], NiS[19,20], MoS_2[21,22] and WS[23,24] have been researched for the possible catalysts to replace the Pt.

Among these metal sulfides, the Cu_2ZnSnS_4 (CZTS) has received much attention in the thin-film solar cells[25-27]. However, only limited literatures reported its use as the CE in DSSCs[28,29]. The elements of quaternary compound, CZTS, are earth abundant, low cost and non-toxic. In addition, it is a direct band gap material[30,31] with an absorption coefficient of 10^4 cm^{-1} in the visible light region[31]; the value of CZTS band gap is affected by the molar composition of CZTS, and lies in a range of 1.4~1.7 eV[30,31]. The physical properties of CZTS depend on its composition and crystal structure[32-34]. Thin film of CZTS, which was studied in quantum dot-sensitized solar cells as the counter electrode, exhibited 3.73% cell efficiency (η) comparing to an η of 2.27% for Pt[28]. Xin *et al.*[29] first reported the CZTS CE using the solution-base synthesis approach, which achieved 3.62% cell efficiency. After selenization, the value of η was significantly increased to 7.37%, which was superior to an η of 7.04% using Pt CE. There are few studies on the electrocatalytic properties of CZTS CE in DSSCs[29,35-37].

In order to optimize the cell performance of DSSCs, it is necessary to explore the influence of the molar ratio of [Cu]/[Zn]+[Sn] on the basic properties of CZTS. In this study, we prepared the CZTS CEs with various [Cu]/[Zn]+[Sn] molar ratios by using the sulfurization of direct-current (DC) magnetron sputtering Cu-Zn-Sn metal alloy. In order to adjust the molar ratio of CZTS samples, the atomic ratio of Cu:Sn:Zn in the precursor was controlled by using various deposition times. The influence of the molar ratio of CZTS CEs on their structure and morphology were characterized by X-ray diffraction pattern (XRD), Raman spectrometer (Raman), energy-dispersive analysis

of X-ray (EDAX), atomic force microscope (AFM), and field–emission scanning electron microscopy (FE-SEM). The electrocatalytic ability and electrochemical properties of the CZTS CEs were investigated by using cyclic voltammetry (CV), electrochemical impedance spectroscopy (EIS), and Tafel plot measurements. The performance of DSSCs, with CZTS and Pt CEs, was verified by *J–V* curves and incident photon–to–current conversion efficiency (IPCE) curves.

Experimental

Materials

Titanium (IV) tetraisopropoxide (TTIP, >98%), dimethyl sulfoxide (DMSO, ≥99.5%), ethanol (EtOH, 99.5%), isopropyl alcohol (IPA, 99.5%), lithium perchlorate ($LiClO_4$, ≥98.0%), Nafion® solution, 1–butyl–3–methyl imidazolium iodide (BMII), 1–ethyl–3–methyl imidazolium tetra-fluoroborate ($EMIBF_4$) and 2–methoxyethanol (≥99.5%) were obtained from Sigma Aldrich. Lithium iodide (LiI, synthetical grade), iodine (I_2, synthetical grade) and poly(ethylene glycol) (PEG, MW~20,000) were obtained from Merck. Acetone (99+%), 4–tert–butylpyridine (tBP, 96%), and tert–butyl alcohol (tBA, 96%) were obtained from Acros. 3–methoxypropionitrile (MPN, 99%) was obtained from Fluka. 1,2–dimethyl–3–propylimidazolium iodide (DMPII) and cis-diisothiocyanato-bis(2,2'-bipyridyl-4,4'-dicarboxylato) ruthenium (II) bis(tetrabutylammonium) (N719 dye) were obtained from Solaronix (S.A., Aubonne, Switzerland). Acetonitrile (ACN, 99.99%), nitric acid (HNO_3, 65% solution in water) was obtained from J. T. Baker.

Preparation of counter electrodes

Indium-doped tin oxide (ITO, 10 Ω $sq.^{-1}$, UR-ITO007-0.7mm, Uni-onward Corp., Taiwan) and fluorine–doped SnO_2 (FTO, TEC-7, 7 Ω $sq.^{-1}$, NSG America, Inc., New Jersey, USA) were cleaned using a neutral cleaner and washed with deionic water, acetone, and isopropanol sequentially. The Pt CE was prepared by DC sputtering on an ITO glass with a thickness of 50 nm. The Cu_2ZnSnS_4 (CZTS) CE was prepared using a direct-current (DC) magnetron sputtering of Cu-Sn (Cu/Sn=52/48 wt%, 99.99%, Summit-Tech) and Zn (99.99%, Summit-Tech) targets. The thicknesses of Cu-Sn and Zn were controlled by using digital quartz controller (Filtech SQM-180). First of all, the cleaned ITO substrates were set in the vacuum chamber which was evacuated to a base pressure of $5x10^{-6}$ torr, high-purity (99.995%) argon gas was used to provide the plasma at a base pressure of $5x10^{-3}$ torr. In order to obtain the same film thickness (1.5 μm) for all samples, the deposition times for Cu-Sn and In were varied to obtain various [Cu]/[Zn]+[Sn] molar ratios in CZTS films. The Cu-Sn metal alloy film was deposited onto ITO using the 2-inch Cu-Sn alloy target with the DC sputtering power of 35 W cm^{-2}. The deposition times of Cu-Sn alloy were set to be 18.0, 17.6, 17.3, 16.5, and 15.5 min for samples (A), (B), (C), (D), and (E), respectively. Sequentially, the Zn metal precursor was deposited on the surface of Cu-Sn alloy layer using the 2-inch Zn metal target with the DC sputtering power of 20 W cm^{-2}. The deposition times of Zn metal were set to be 4.5, 4.7, 4.9, 5.3 and 5.8 min for samples (A), (B), (C), (D), and (E), respectively. Therefore, the Cu-Sn alloy layer can be well-covered with the Zn metal to prevent the formation of SnS impurities during the sulfurization process[38]. The two-step post-thermal sulfurization process for the Cu-Sn-Zn metal precursor was carried out in a container with 0.5 g sulfur powder. An outer evacuated quartz tube was used for a two-stage annealed process under a vacuum condition of around $5x10^{-3}$ torr. In the first sulfurization stage, the metal precursors and sulfur powders were annealed at 440 °C for 30 min. Then the formation of Cu_2ZnSnS_4 on the substrate was carried out at the second sulfurization stage by holding at 560 °C for 30 min [39,40].

Preparation of photoanode and DSSCs

The 0.5 M TTIP in 0.1 M nitric acid aqueous solution was constant stirred and heated up to 88 °C simultaneously for 8 h, and sequentially heating to 240 °C for 12 h in an autoclave (PARR 4540, U.S.A.). The TiO_2 paste for transparent layer (TL) was concentrated the TiO_2 to 8 wt% by adding 2 wt% of PEG. The other TiO_2 paste for scattering layer (SL) was provided by adding 8 wt% commercial light scattering TiO_2 particles (ST-41, 200 nm, Ishihara Sangyo, Ltd., Japan) into TL paste. FTO conducting surface was first treated by spin coating a 100 nm compact layer using a solution of TTIP in 2–methoxyethanol (weight ratio of 1:3). A 20 μm porous TiO_2 film containing 15 μm TL and 5 μm SL was coated on the treated FTO glass by the doctor blade technique, and the TiO_2 film was sintered at 500 °C for 30 min in an air atmosphere. After the annealing process, the TiO_2 photoanode was reduced to 0.16 cm^2 as the active area and immersed in 5×10^{-4} M to adsorb N719 dye at room temperature for 24 h. The TiO_2 photoanode was coupled with the CE and the distance between these two electrodes was fixed and sealed by heating a 60 μm–thick Surlyn® (SX1170–60, Solaronix S.A., Aubonne, Switzerland). The electrolyte, which consisted of 0.6 M DMPII, 0.1 M LiI, 0.05 M I_2, and 0.5 M TBP in MPN/ACN (volume ratio = 1:1), was injected into the gap between these two electrodes by capillarity.

Characterization of counter electrodes and DSSCs

The compositions of the samples were analyzed using a EDAX and the surface morphologies of CZTS CEs were observed by field–emission scanning electron microscopy (FE–SEM, JEOL JSM 6700F). The phase formation and crystallographic study of samples on glass substrates were investigated using an X-ray diffractometer (Siemens D5005) with CuK_α (λ = 1.5405 Å) and Raman spectrometer (Protrustech, UniRaman, YAG laser 523 nm). The X-ray diffraction (XRD) patterns were recorded in the 2θ range of 10-80°. The roughness of composite CZTS CE was observed by atomic force microscope (AFM, Park Systems XE70). The catalytic abilities of the CEs for I^-/I_3^- redox couple and electrochemical properties can be estimated through cyclic voltammetry (CV), Tafel plot, and EIS. The CV curve was measured with a three–electrode electrochemical system in an ACN solution, containing 10.0 mM I^-, 1.0 mM I_2, and 0.1 M $LiClO_4$. The Pt or composite CZTS film was used as the working electrode, and the Pt foil and Ag/Ag^+ electrode were used as the counter and reference electrode, respectively. Tafel plot and EIS spectra of symmetric cells of different CEs were measured by the potentiostat/galvanostat (PGSTAT 30, Autolab, Eco–Chemie, Utrecht, the Netherlands) equipped with an FRA2 module. Cell

conversion efficiencies (η) of DSSCs with different CEs were measured by the potentiostat/galvanostat under 100 mW cm^{-2} light illumination by a solar simulator (XES–301S, AM1.5G, San–Ei Electric Co., Ltd., Osaka, Japan). The incident light intensity was calibrated with a standard Si cell (PECSI01, Peccell Technologies, Inc., Kanagawa, Japan). IPCE curves of DSSCs were obtained by potentiostat/galvanostat and a class A quality solar simulator (PEC–L11, AM1.5G, Peccell Technologies, Inc., Kanagawa, Japan) equipped with a monochromator (model 74100, Oriel Instrument, California, USA). The incident radiation flux (φ) was obtained using an optical detector (model 71580, Oriel Instrument, California, USA) and a power meter (model 70310, Oriel Instrument, California, USA).

Results and discussion

Composition and crystalline characteristics of various CZTS composite films

The atomic percentages of Cu, Zn, Sn, and S in various CZTS CEs were obtained from the EDAX analysis, which is summarized in Table 1. The Zn-based[41] and Sn-based[42,43] thin films as the CE materials have been proposed for use in the DSSCs and their catalytic ability has been confirmed. There are some literatures about doping the Cu-based material to increase the electric conductivity[44,45] and the cell performance. In a CZTS thin film, Cu acts as the key element in the composite due to its high conductivity.

By reducing the deposition time of Cu-Sn alloy, the Cu content in CZTS CEs was decreased from 30.41 to 22.30%, namely from samples (A) to (E). The over-doped Cu content would lead to the formation of $Cu_{2-x}S$ impurity phase[46], which can increase the charge-transfer resistance of the CE. Therefore, the [Cu]/[Zn]+[Sn] molar ratio can largely affect the physical properties such as conductivity, surface morphology, and cell efficiency. From the EDAX analysis, sample (C) nearly corresponded to the stoichiometric element of Cu_2ZnSnS_4.

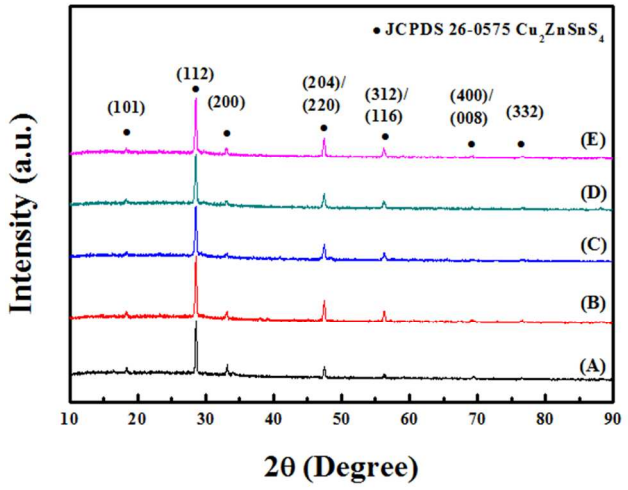

Fig. 1 X-ray diffraction patterns of samples with various molar ratios of CZTS CEs.

The ideal stoichiometric molar ratio of Cu_2ZnSnS_4 is [Cu]:[Zn]:[Sn]:[S]=2:1:1:4, therefore the atomic ratio of sulfur has to approach 50% to avoid the unfavorable sulfur deficient[47-48]. In Table 1, all samples with the [S]/Metal molar ratios are in the range of 0.95-1.02, which reach nearly 50%. Therefore, there are no apparent sulfur defects in all samples. In addition, X-ray photoelectron spectroscopy (XPS, Thermo Scientific Theta Probe, UK) spectra of the CZTS CEs are collected to confirm the EDAX results. As summarized in Table S1, similar results can be concluded from both EDAX and XPS analyses.

Table 1 EDAX analysis of the composite CZTS CEs on the substrates.

CEs	Molar % of CZTS				[Cu]/[Zn]+[Sn]	[S]/Metal
	Cu	Zn	Sn	S		
(A)	30.41	6.84	14.13	48.62	1.45	0.95
(B)	26.61	9.62	13.84	49.93	1.13	1.00
(C)	24.45	11.86	13.44	50.24	0.97	1.01
(D)	23.39	12.79	13.25	50.57	0.90	1.02
(E)	22.30	15.11	13.00	49.59	0.79	0.98

Fig. 1 shows the XRD patterns of samples after the sulfurization process of metal alloys. The peak at 2θ angles of 18.2°, 28.5°, 33.0°, 47.3°, 56.9°, 69.2°, and 76.4° correspond to the crystal planes of (101), (112), (200), (204/220), (312/116), (400/008), and (332), respectively, for the kesterite Cu_2ZnSnS_4 phase without clear impurities such as Cu_xS. According to the literature, the diffraction peaks of the Cubic-ZnS and the cubic-Cu_2SnS_3 are almost the same as the kesterite phase Cu_2ZnSnS_4[50,51]. In order to confirm the crystal phases of CZTS CEs, the Raman spectrometer was used to characterize the crystalline phases. The Raman studies showed three bands at 283 cm^{-1}, 329 cm^{-1} and 368 cm^{-1} in Fig. 2. In fact, the most prominent peaks for a Cu_2ZnSnS_4 thin film were found at 288~289 cm^{-1}, 338~339 cm^{-1} and 370~372 cm^{-1} in literature[50]. Therefore, all CZTS CEs show a dominant Cu_2ZnSnS_4 crystal phase with a minor impurity phase of Cu_2SnS_3, and thereby they can be considered as the composite materials.

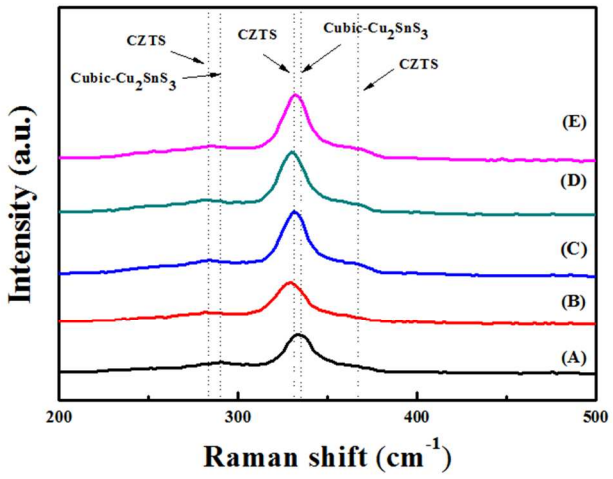

Fig. 2 Raman spectra of CZTS CEs with the various molar ratios.

Morphology and microstructures of the various CZTS composite films

FE–SEM and AFM images were used to observe the microstructures of the samples on the ITO substrates. Fig. 3 shows the SEM images of the CZTS CEs; the inset of each image gives the pertinent high-resolution SEM image of each CZTS CE. Except for sample (A), the grain size becomes larger with the increasing molar ratio of [Cu]/[Zn]+[Sn] in the samples, indicating that Cu would enhance the grain growth[25]. In the case of sample (A), the over-doped Cu content would lead to the coexistence of the secondary phase and ternary phase with high concentration of defect clusters, as compared to the other samples. The coexisted phases would prevent the grain from further growing, thus leading to nonuniform grain size. Therefore, the film composed of aggregated particles in sample (A) becomes more smooth. As the [Zn] content is increased, the crystal structure of the film would change from particle to plate[52]. Thus, the structural properties were predominantly influenced by both the [Cu] and [Zn] contents. Since sample (C) has less defects comparing to other samples, this would give rise to a more uniform grain with a dense surface, as shown by a plane view FE-SEM image in Fig. S3.

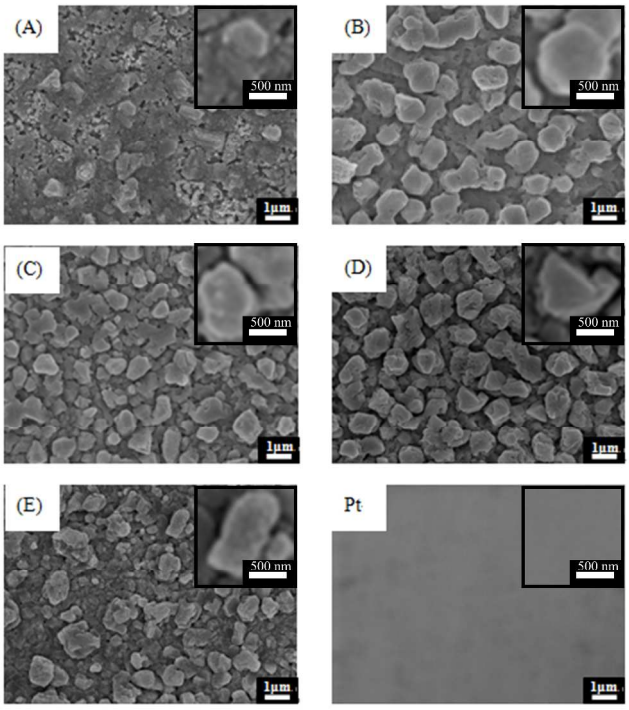

Fig. 3 Plane view FE-SEM images of CZTS CEs with various molar ratios.

Fig. 4 shows AFM images of samples on the ITO substrates. From the AFM images, the root mean square roughness (R_{rms}) was found to be 188.0±0.4, 246.4±0.2, 275.9±0.3, 180.3±0.2 and 153.2±0.5 nm for samples (A), (B), (C), (D), and (E), respectively. When the [Zn] or [Cu] content was increased too much, the surface morphology showed many plate-like particles or aggregations of particles covering on the surface, respectively, thus giving a small surface roughness. Among all the CZTS films, sample (C) shows the largest R_{rms} value, which implies its largest electrocatalytic surface area for I_3^- reduction.

Photovoltaic performance of DSSCs with various CEs

Photocurrent density-voltage *(J-V)* characteristics of the DSSCs with various molar ratios of CZTS CEs are shown in Fig. 5a and the photovoltaic parameters are listed in Table 2. The open-circuit voltage (*Voc*) of all samples is similar, indicating that the value of *Voc* is not affected by the molar ratio. The optimized composite CZTS achieved 7.94% cell performance with higher V_{OC}, Fill factor (*FF*), and short-circuit current density (J_{sc}) being 740.5 mV, 0.62 and 17.2 mA cm^{-2}, respectively. Although the standard DSSC with Pt as the CE had the cell efficiency of 8.55% under the same measurement condition, the low-cost CZTS exhibits only a slightly lower cell efficiency, thus possessed some potential to replace the Pt CE. Variable elementary defects in CZTS CEs, such as Cu or Zn defects, can trap the electrons and lower the conductivity of the thin film, so that the *FF* of their DSSCs are poor. Moreover, the J_{sc} can be increased by the larger surface area of sample (C), which can be verified by the larger surface roughness of 275.9 nm obtained from AFM measurement.

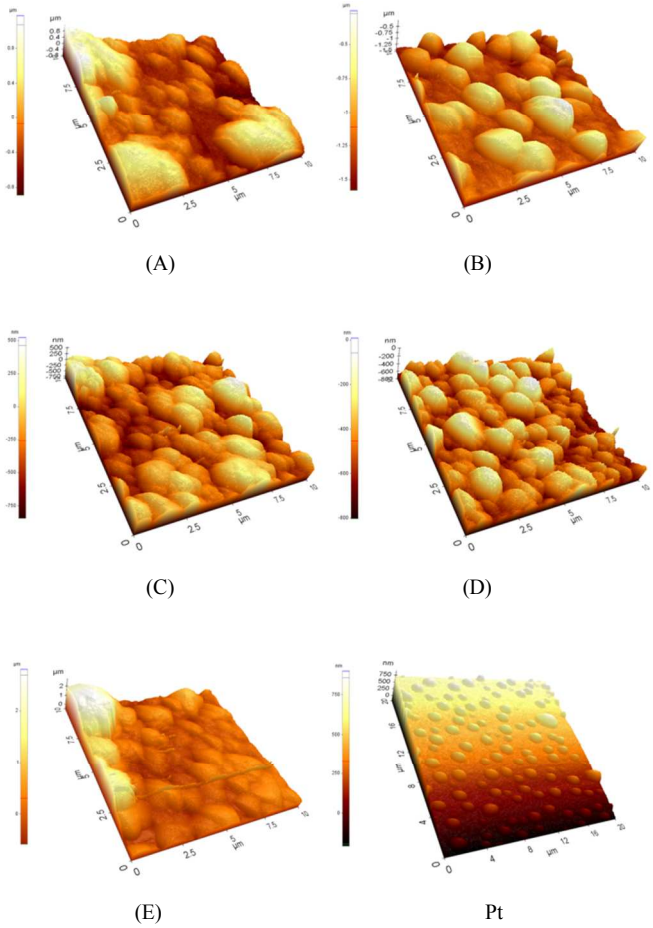

Fig. 4 AFM micrographs of CZTS CEs with various molar ratios.

The EDAX and XRD indicate that sample (C) corresponded to Cu_2ZnSnS_4 phase and no additional elementary defects to trap the

electrons, so these results show sample (C) is a better electro-catalyst comparing to other samples. The large roughness of CZTS CEs is beneficial for its enhancement of electrochemical activity. The surface morphology of Cu-rich or Zn-rich are more uniform than others, so the behavior of J_{sc} decreased from 17.2 mA cm^{-2} to 12.2 mA cm^{-2}. The lower values of J_{sc} of the DSSC with the composite films are in consistency with the lower electrocatalytic activity of the films.

On the other hand, the DSSC with sample (C) as the counter electrode was subjected to an at-rest long-term stability test, as shown in the electronic supplementary information (Fig. S1). A proper binary ionic liquid electrolyte, containing 0.2 M I_2 and 0.5 M TBP in a mixture solvent of BMII and $EMIBF_4$ (volume ratio = 65:35), was used for the test. After one month, the normalized cell efficiency with sample (C) CE maintains up to 90% of its initial value, which supports the good long-term stability of the CZTS CE and its promising electrocatalytic ability as the CE for DSSCs.

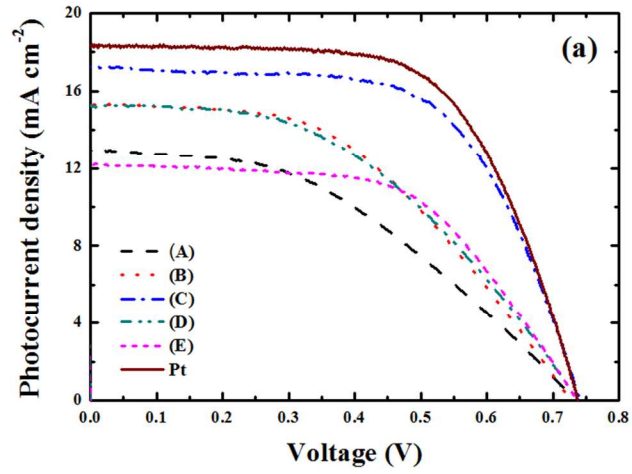

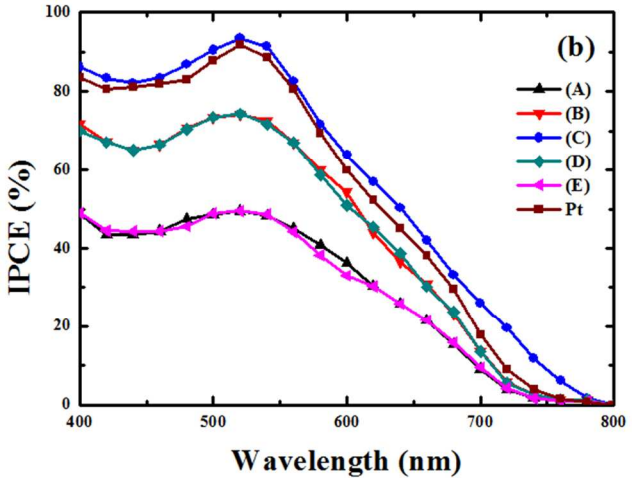

Fig. 5 (a) Photocurrent density–voltage curves of DSSCs with various CEs, measured at 100 mW cm^{-2} (AM 1.5G) light intensity, (b) IPCE curves of DSSCs with various CEs.

IPCE of DSSCs

Fig. 5b shows the IPCE spectra of the DSSCs coupling with different CEs. The IPCE curves corresponding to sample (C) and Pt CEs are comparable. The higher IPCE value yields the higher J_{sc} value of the DSSC, which implies the larger surface area of the CE. All of the IPCE values are agreed with the J_{sc} values.

Cyclic voltammetry analysis of various CEs

The CV measurement can be used for investigating the reaction kinetics and electrocatalytic abilities of the CZTS CEs at various molar ratios. Fig. 6 displays the CV curves of I^-/I_3^- redox couple by using a three-electrode electrochemical system. The major reduction at the counter electrode can be represented as:

$$I_3^- + 2e^- \rightarrow 3I^- \quad (1)$$

Sample (C) composite shows the higher redox current densities than the other composite, which implied that sample (C) thin film possessed better electrocatalytic activity for I^-/I_3^- redox reaction.

Table 2 Photovoltaic parameters of the DSSCs with various CZTS CEs and Pt CE, measured at 100 mW cm^{-2} (AM 1.5G) light intensity.

CEs	η (%)	V_{OC} (mV)	J_{sc} (mA cm^{-2})	*FF*	R_{rms} (nm)
(A)	4.01	732.1	12.9	0.42	188.0
(B)	5.23	726.2	15.3	0.47	246.4
(C)	7.94	740.5	17.2	0.62	275.9
(D)	5.16	738.1	15.3	0.46	180.3
(E)	5.16	736.2	12.2	0.57	153.2
Pt	8.55	736.1	18.3	0.64	259.2

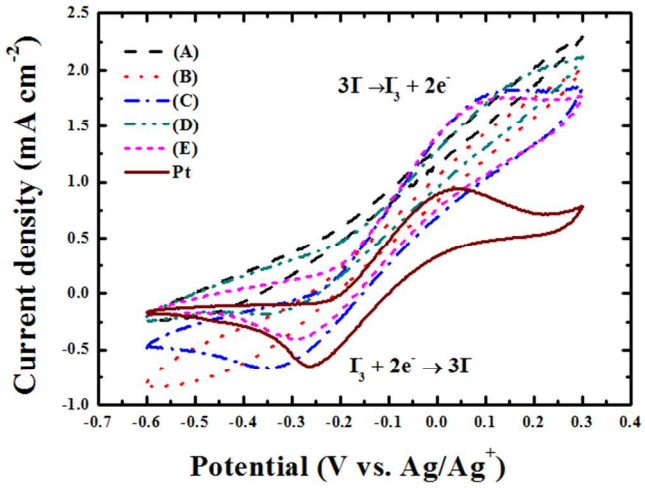

Fig. 6 CV of various CZTS CEs, with an electrolyte of 10.0 mM LiI, 1.0 mM I_2, and 0.1 M $LiClO_4$ in ACN.

The anodic peak current density (J_{pa}), the cathodic peak current density (J_{pc}) and the peak separation (ΔE_p) are listed in Table 3. We observe that the cathodic peak current density of sample (C)

shows nearly the same as that of the Pt CE. The cathodic and anodic peak current densities (J_{pc} and J_{pa}) are determined by the difference between the maximum peak current density and the baseline of charging current density[53]. The high value of the J_{pc} shows the better electrocatalytic ability of a CE for I_3^- reduction.

Table 3 CV parameters for different CEs in ACN solution containing 10.0 mM LiI, 1.0 mM I_2, and 0.1 M $LiClO_4$ at a scan rate of 50 mV s^{-1}.

CEs	J_{pc} (mA cm^{-2})	J_{pa} (mA cm^{-2})	ΔE_p (V)
(A)	0.15	0.10	0.60
(B)	0.20	0.14	0.57
(C)	0.35	0.30	0.42
(D)	0.23	0.20	0.50
(E)	0.25	0.30	0.36
Pt	0.42	0.36	0.35

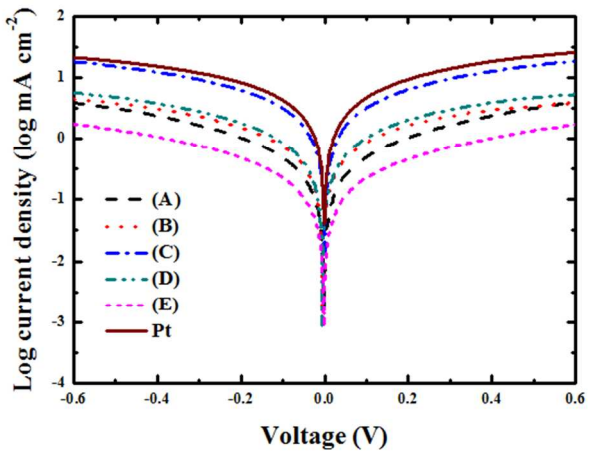

Fig. 7 Tafel polarization curves of various CEs.

We observe also that the value of J_{pc} for sample (C) is larger than other CZTS CEs, indicating that it exhibits the highest electrocatalytic ability among all of the CZTS CEs. The lower ΔE_p represents the higher kinetic ability for I_3^- reduction. And sample (C) composite CE possessed comparable J_{pc} and ΔE_p values to those of Pt CE. From the CV results, we conclude that the similar J_{pc} and ΔE_p values would directly lead to the higher J_{sc} values of the DSSCs.

To further confirm the long-term stability of sample (C) CE in the I^-/I_3^- electrolyte, we executed a long-term CV analysis under continuous 100 cycles scanning, which is shown in the electronic supplementary information (Fig. S2). In Fig. S2a, the anodic and cathodic peak current densities (J_{pa} and J_{pc}) of sample (C) show constant amplitudes after 100 cycles, which implies its good long-term stability. Fig. S2b plots the values of J_{pa} and J_{pc} as a function of the cycle number. Those values remain almost the same up to 100 cycles, suggesting that the CZTS composite thin film is stable and not corroded in the I^-/I_3^- electrolyte.

Tafel and EIS analyses of optimized CZTS and Pt CEs

In order to further confirm the electrocatalytic abilities of CZTS CEs, we use Tafel polarization curve measurement and EIS analysis. The interfacial charge-transfer properties in the symmetric cell could be studied by Tafel polarization curve

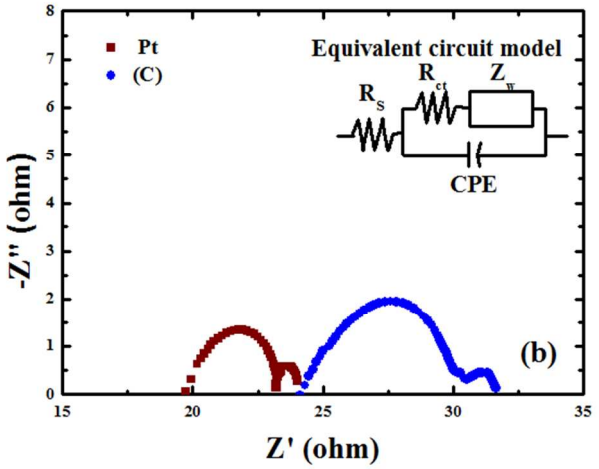

measurement. Tafel polarization curves of the symmetric cell based on all of samples are shown in Fig. 7.

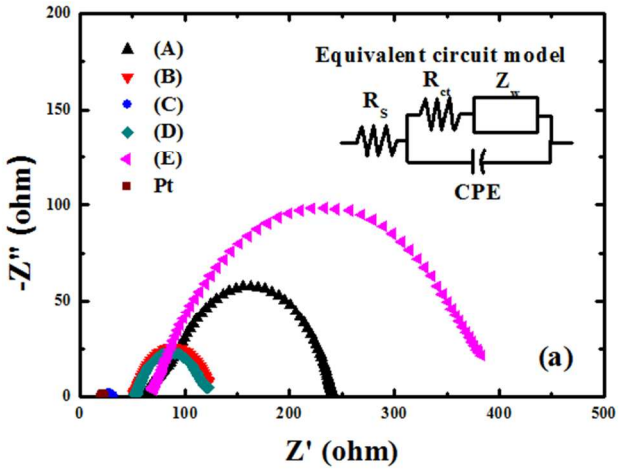

Fig. 8 (a) Electrochemical impedance spectra of various CEs, **(b)** Electrochemical impedance spectra of CZTS and Pt CEs.

The exchange current density (J_o) can be calculated from the intercept of the linear fitting line of anodic and cathodic data. The charge transfer resistance (R_{ct}) for the various CEs can be calculated by eqn (2):

$$J_0 = \frac{RT}{nFR_{ct}} \quad (2)$$

where T is the absolute temperature, R is the gas constant, F is the Faraday constant, n is the total number of electrons involved in the reaction, and R_{ct} is the charge transfer resistance. In Table 4, sample (C) and Pt CE show the similar R_{ct} value, suggesting that sample (C) possesses superior electrocatalytic ability. The R_{ct} value can be affected by two key parameters: one is the surface

area, the other is the electrocatalytic ability, which are determined by the roughness (R_{rms}) and cathodic peak current density (J_{pc}), respectively. The R_{rms} value shows the tendency of (C) > (B) > (A) > (D) > (E), however the J_{pc} value shows the tendency of (C) > (E) > (D) > (B) > (A). Some disagreements appear in the cases of films of (D) and (E); this may be attributed to the overdose Cu-defects, which can trap the electrons thus enhance the resistance at the CE/electrolyte interface. Therefore, the R_{ct} value shows the tendency of (C) > (D) > (B) > (A) > (E).

The EIS spectra of symmetric cells based on CZTS CE and Pt are shown in Fig. 8. The radius of left semicircle can be attributed to the charge transfer resistance (R_{ct}) of the CE/electrolyte interface. On the other hand, the right semicircle is corresponded to the resistance for diffusion process in the electrolyte. The CZTS CE is fabricated using sputtering can serve better adhesion to the substrate and enhance the charge transfer ability. The lower R_{ct} value influenced on the electron transfer from the CE to the I_3^-, thus lead to the higher J_{sc} and FF[54], which are consistent with the R_{ct} values obtained from Tafel polarization results. In Fig. 8, the R_{ct} value of sample (C) and Pt CEs are 2.93 and 1.75 Ω cm^2, respectively. From which, sample (C) shows a comparable electrocatalytic ability to Pt. Moreover, the values of the nonideal frequency dependent capacitance at the CE/electrolyte interface, represented by the constant phase element (CPE), are calculated for all samples by using the Z-view software[55,56]. The higher CPE value represents the larger surface area of the CE[56]. In Table 4, CPE values show the tendency of (C) > (A) > (D) > (E) > (B), which agree well with the results obtained from the FE-SEM and AFM analyses. In brief, sample (C) shows the comparable electrocatalytic ability and active surface area to those of Pt, which demonstrates that sample (C) is a promising candidate to replace Pt as CEs in DSSCs.

Table 4 Electrochemical parameters of Pt and other CZTS CEs.

CEs	R_s [a] (Ω cm^2)	R_{ct} [a] (Ω cm^2)	CPE (μF cm^{-2})	R_{ct} [b] (Ω cm^2)
(A)	65.37	88.43	0.35	88.45
(B)	51.74	39.05	0.05	39.06
(C)	24.11	2.93	2.99	2.94
(D)	53.33	35.05	0.14	35.16
(E)	69.19	182.68	0.06	182.72
Pt	19.73	1.75	11.22	1.73

[a] Values obtained from EIS; [b] Values obtained from Tafel plot.

Conclusions

A highly efficient counter electrode based on low-cost quaternary CZTS was fabricated successfully. The influence of molar ratio of CZTS CEs on the structural and morphological properties was investigated. All of the CZTS CEs revealed the kesterite Cu_2ZnSnS_4 phase. The Cu and Zn elements predominantly influenced the grain size and morphology. The adjustment of molar ratio of CZTS is very important to obtain the desired properties, leading to optimize the cell performance of DSSCs. The near-stoichiometric composition of CZTS CE showed the better electrocatalytic ability than the other composites. This resulted in high electrocatalytic activity for the I^-/I_3^- redox reaction, which is similar to that of the Pt CE. The DSSC coupled with the optimized CZTS CE achieved a cell efficiency of 7.94% with V_{OC} of 740.5 mV, J_{sc} of 17.2 mA cm^{-2}, and FF of 0.62, which is comparable to the DSSC with Pt CE (8.55%). Consequently, several advantages, such as low-cost material, possible large scale production[57-59], and high solar-to-electrical power conversion efficiency of 7.94%, can be achieved by applying the CZTS CE in DSSCs. In this study, we demonstrated the CZTS is a potential substitute to replace the Pt CE.

Acknowledgements

This work was sponsored by the Ministry of Science and Technology of Taiwan, under grant number of 102-2221-E-002-186-MY3.

Notes and references

[a]*Department of Chemical Engineering, National Taiwan University, No.1, Sec. 4, Roosevelt Road, Taipei 10617, Taiwan. Fax: +886–2–2362–3040; Tel: +886–2–2366–0739; E–mail:kcho@ntu.edu.tw*

[b]*Department of Chemical and Materials Engineering, Chang Gung University, No. 259 Wen-Hwa 1st Road, Kwei-Shan, Tao-Yuan 333, Taiwan. Fax: +886–3–211–8668; Tel.: +886–3–211–8800 ext 3353; E-mail: kwcheng@mail.cgu.edu.tw*

[c]*Institute of Polymer Science and Engineering, National Taiwan University, No. 1, Sec. 4, Roosevelt Road, Taipei 10617, Taiwan. Fax: +886–2–2362–3040; Tel: +886–2–2366–0739; E–mail:kcho@ntu.edu.tw*

† Electronic supplementary information (ESI) available. See DOI:10.1039/b000000x/

‡ These authors contributed equally.

* Corresponding author.

1. H. Wang, W. Wei and Y. H. Hu, *J. Mater. Chem. A*, 2013, **1**, 6622.
2. G. Wang, W. Xing and S. Zhuo, *Electrochim. Acta*, 2013, **92**, 269.
3. J. Yang, C. Bao, J. Zhang, T. Yu, H. Huang, Y. Wei, H. Gao, G. Fu, J. Liu and Z. Zou, *Chem. Commun.*, 2013, **49**, 2028.
4. X. Zheng, J. Guo, Y. Shi, F. Xiong, W. H. Zhang, T. Ma and C. Li, *Chem. Commun.*, 2013, **49**, 9645.
5. S. Tai, C. F. Chang, W. C. Liu, J. H. Liao and J. Y. Lin, *Electrochim. Acta*, 2013, **107**, 66.
6. J. Ma, L. Zhou, C. Li, J. Yang, T. Meng, H. Zhou, M. Yang, F. Yu and J. Chen, *J. Power Sources*, 2014, **247**, 999.
7. W. Zeng, G. Fang, T. Han, B. L. N. Liu, D. Zhao, Z. Liu, D. Wang, X. Zhao and D. Zou, *J. Power Sources*, 2014, **245**, 456.
8. C. Y. Lin, C. H. Shan, S. Y. Tsai, K. W. Lin, C. S. Chang, and S. S. C. Forest, *J. Appl. Phys.*, 2013, **114**, 014503.
9. J. Y. Lin, W. Y. Wang and Y. T. Lin, *Surf. Coat. Technol.*, 2013, **231**, 171.
10. N. Jeon, D. K. Hwang, Y. S. Kang, S. S. Im and D. W. Kim, *Electrochem. Commun.*, 2013, **34**, 1.
11. Z. Yan and L. Zhang, *J. Appl. Electrochem.*, 2013, **43**, 605.
12. M. Wu, Y. Wang, X. Lin, W. Guo, K. Wu, Y. N. Lin, H. Guo and T. Ma, *J. Mater. Chem. A*, 2013, **1**, 9672.
13. Y. C. Wang, D. Y. Wang, Y. T. Jiang, H. A. Chen, C. C. Chen, K. C. Ho, H. L. Chou and C. W. Chen, *Angew. Chem. Int. Ed.*, 2013, **52**,

6694.
14. Y. Hu, Z. Zheng, H. Jia, Y. Tang and L. Zhang, *J. Phys. Chem. C*, 2008, **112**, 13037.
15. Y. C. Wang, D. Y. Wang, Y. T. Jiang, H. A. Chen, C. C. Chen, K. C. Ho, H. L. Chou and C. W. Chen, *Angew. Chem. Int. Ed.*, 2013, **52**, 6694.
16. H. Yuan, J. Lu, X. Xu, D. Huang, W. Chen, Y. Shen and M. Wang, *J. Electrochem. Soc.*, 2013, **160**, H624.
17. F. D. Rossi, L. D. Gaspare, A. Reale, A. D. Carlo and T. M. Brown, *J. Mater. Chem. A*, 2013, **1**, 12941.
18. J. Y. Lin, Y. T. Tsai, S. Y. Tai, Y. T. Lin, C. C. Wan, Y. L. Tung and Y. S. Wu, *J. Electrochem Soc.*, 2013, **160**, D46.
19. Z. Li, F. Gong, Gang Zhou and Z. S. Wang, *J. Phys. Chem. C*, 2013, **117**, 6561.
20. W. Zhao, X. Zhu, H. Bi, H. Chi, S. Sun and F. Huang, *J. Power Sources*, 2013, **242**, 28.
21. G. Yue, W. Zhang, J. Wu and Q. Jiang, *Electrochim. Acta*, 2013, **112**, 655.
22. S. Y. Tai, C. J. Liu, S. W. Chou, F. S. S. Chien, J. Y. Lin and T. W. LIn, *J. Mater. Chem.*, 2012, **22**, 24753.
23. J. Wu, G. Yue, Y. Xiao, M. Huang, J. Lin, L. Fan, Z. Ln and J. Y. Lin, *ACS Appl. Mat. Interfaces*, 2012, **4**, 6530.
24. L. Cheng, Y. Hou, B. Zhang, S. Yang, J. W. Guo, L. Wu and H. G. Yang, *Chem. Commun.*, 2013, **49**, 5949.
25. X. Jiang, L. X. Shao, J. Zhang, D. Li, W. Xie, C. W. Zou and J. M. Chen, *Surf. Coat. Technol.*, 2013, **228**, s408.
26. M. Xie, D. Zhuang, M. Zhao, B. Li, M. Cao and J. Song, *Vacuum*, 2014, **101**, 146.
27. R. Ishinoa, K. Fukushima and T. Minemoto, *Curr. Appl. Phys.*, 2013, **13**, 1861.
28. J. Xu, X. Yang, Q. D. Yang, T. L. Wong and C. S. Lee, *J. Phys. Chem. C,* 2012, **116**, 19718.
29. X. Xin, M. He, W. Han, J. Jung and Z. Lin, *Angew. Chem. Int. Ed.*, 2011, **50**, 11739.
30. H. Katagiri, N. Sasaguchi, S. Hando, S. Hoshino, J. Ohashi and T. Yokota, *Sol. Energy Mater. Sol. Cells*, 1997, **49**, 407.
31. H. Katagiri, K. Saitoh, T. Washio, H. Shinohara, T. Kurumadani and S. Miyajima, *Sol. Energy Mater. Sol. Cells*, 2001, **65**, 141.
32. S. Chen, A. Walsh, X. G. Gong and S. H. Wei, *Adv. Mater.*, 2013, **25**, 1522.
33. S. Chen, A. Walsh, J. H. Yang, X. G. Gong, L. Sun, P. X. Yng, J. H. Chu and S. H. Wei, *Phys. Rev. B*, 2011, **83**, 125201.
34. T. Tanaka, A. Yoshida, D. Saiki, K. Saito, Q. Guo, M. Nishio, T. Yamaguchi, *Thin Solid Films*, 2010, **518**, S29.
35. J. Kong, Z. J. Zhou, M. Li, W. H. Zhou, S. J. Yuan, R. Y. Yao, Y. Zhao and S. X. Wu, *Nanoscale Res. Lett.*, 2013, **8**, 464.
36. Z. Hou, Z. Zhou, S. Yuan, W. Zhou, S. Wu and D. Xue, *Sci. Adv. Mater.*, 2013, **5**, 1764
37. Z. Tong, Z. Su, F. Liu, L. Jiang, Y. Lai, J. Li and Y. Liu, *Mater. Lett.,* 2014, **121**, 241.
38. A. Fairbrother, X. Fontané, V. I. Roca, M. E. Rodríguez, S. L. Marinoa, M. Placidi, L. C. Barrio, A. P. Rodríguez and E. Saucedo, *Sol. Energy Mater. Sol. Cells*, 2013, **112**, 97.
39. H. Yoo, J. Kim and L. Zhang, *Curr. Appl. Phys.*, 2012, **12**, 1052.
40. F. Hergert and R. Hock, *Thin Solid Films*, 2007, **515**, 5953.
41. D. P. Joseph, S. Ganesan, M. Kovendhan, S. A. Suthanthiraraj, P. Maruthamuthu and C. Venkateswaran, *Phys. Status Solidi A*, 2011, **208**, 2215.
42. S. Chappel and A. Zaban, *Sol. Energy Mater. Sol. Cells*, 2002, **71**, 141.
43. K. Li, Y. Luo, Z. Yu, M. Deng, D. Li and Q. Meng, *Electrochem. Commun.*, 2009, **11**, 1346.
44. F. Huang, J. Xu, D. Chen and Y. Wang, *Nanotechnology*, 2012, **23**, 425604.
45. C. Liu, Z. Liu, J. Li, Y. Li, J. Han, Y. Wang, Z. Liu and J. Ya, *Microelectron. Eng.*, 2013, **103**, 12.
46. A. Nagoya and R. Asahi, *Phys. Rev. B*, 2010, **81**, 113202.
47. V. Kosyak, N. B. Mortazavi Amiri, A. V. Postnikov and M. A. Scarpulla, *J. Appl. Phys.*, 2013, **114**, 124501-1.
48. C. Platzer-Björkman, J. Scragg, H. Flammersberger, T. Kubart and M. Edoff, *Sol. Energy Mater. Sol. Cells*, 2012, **98**, 110.
49. S. M. Pawar, A. I. Inamdar, B. S. Pawar, K. V. Gurav, S. W. Shin and X. Yanjun, *Mater. Lett.*, 2014, **118**, 76.
50. P. A. Fernandes, P. M. P. Salome and A. F. d. Cunha, *J. Alloy. Compd.*, 2011, **509**, 7600.
51. S. W. Sin, S. M. Pawar, C. Y. Park, J. H. Yun, J. H. Moon, J. H. Kim and J. Y. Lee, *Sol. Energy Mater. Sol. Cells*, 2011, **95**, 3202.
52. K. W. Cheng, Y. H. Cheng and M. S. Fan, *Int. J. Hydrogen Energy*, 2012, **37**, I3763.
53. A. Bard and L. Faulkner, Electrochemical Methods: Fundamental and Applications, John Wiley & Sons, Inc., 2nd edn, 2001.
54. T. Ma, X. Fang, M. Akiyama, K. Inoue, H. Noma and E. Abe, *J. Alloy. Compd.*, 2004, **574**, 77.
55. N. T. Q. Hoa, V. D. Dao, H. S. Choi, *J. Mater. Sci.*, 2014, **49**, 4973.
56. J. Y. Lin, J. H. Liao, S. W. Chou, *Electrochim. Acta*, 2011, **56**, 8818.
57. M. G. Sousa, A. F. da Cunha, P. M. P. Salomé, P. A. Fernandes, J. P. Teixeira and J. P. Leitão, *Thin Solid Films*, 2012, **535**, 27.
58. F. Jiang, H. Shen, W. Wang and L. Zhang, *Appl. Phys. Express*, 2011, **4**, 074101-1.
59. H. Yoo and J. Kim, *Thin Solid Films*, 2010, **518**, 6567.

Preparation of Copper Zinc Tin Sulfide as the Catalytic Materials for Counter Electrodes in Dye-Sensitized Solar Cells

Miao-Syuan Fan,[‡a] Jian-Hao Chen,[‡b] Chun-Ting Li,[a] Kong-Wei Cheng,[*b] and Kuo-Chuan Ho[*ac]

[a] *Department of Chemical Engineering, National Taiwan University, Taipei 10617, Taiwa*

[b] *Department of Chemical and Materials Engineering, Chang Gung University, Taoyuan 33302, Taiwan*

[c] *Institute of Polymer Science and Engineering, National Taiwan University, Taipei 10617, Taiwan*

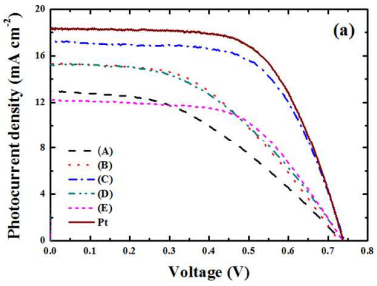

A dye-sensitized solar cell (DSSC) with synthesized Cu_2ZnSnS_4 catalytic counter electrode (CE) exhibits a cell efficiency of 7.94%, which shows comparable performance to that of Pt CE (8.30%).